Characterization of bending losses for curved plasmonic nanowire waveguides

Dirk Jan Dikken, Marko Spasenović*, Ewold Verhagen, Dries van Oosten, and L. (Kobus) Kuipers

Center for Nanophotonics, FOM institute for Atomic and Molecular Physics (AMOLF), Science Park 104, 1098 XG, Amsterdam, The Netherlands
**marko@amolf.nl*

Abstract: We characterize bending losses of curved plasmonic nanowire waveguides for radii of curvature ranging from 1 to 12 μm and widths down to 40 nm. We use near-field measurements to separate bending losses from propagation losses. The attenuation due to bending loss is found to be as low as 0.1 μm^{-1} for a curved waveguide with a width of 70 nm and a radius of curvature of 2 μm. Experimental results are supported by Finite Difference Time Domain simulations. An analytical model developed for dielectric waveguides is used to predict the trend of rising bending losses with decreasing radius of curvature in plasmonic nanowires.

OCIS codes: (250.5403) Plasmonics; (230.7370) Waveguides; (250.5300) Photonic integrated circuits.

References and links

1. S. A. Maier, "Plasmonics – Towards Subwavelength Optical Devices," Curr. Nanosci. **1**(1), 17–22 (2005).
2. J. Homola, S. S. Yee, and G. Gauglitz, "Surface plasmon resonance sensors: review," Sens. Actuactors B **54**(1-2), 3–15 (1999).
3. D. E. Chang, A. S. Sørensen, P. R. Hemmer, and M. D. Lukin, "Strong coupling of single emitters to surface plasmons," Phys. Rev. B **76**(3), 035420 (2007).
4. J. A. H. van Nieuwstadt, M. Sandtke, R. H. Harmsen, F. B. Segerink, J. C. Prangsma, S. Enoch, and L. Kuipers, "Strong modification of the nonlinear optical response of metallic subwavelength hole arrays," Phys. Rev. Lett. **97**(14), 146102 (2006).
5. Y. Vlasov, W. M. J. Green, and F. Xia, "High-throughput silicon nanophotonic wavelength-insensitive switch for on-chip optical networks," Nat. Photonics **2**(4), 242–246 (2008).
6. D. M. Beggs, T. P. White, L. O'Faolain, and T. F. Krauss, "Ultracompact and low-power optical switch based on silicon photonic crystals," Opt. Lett. **33**(2), 147–149 (2008).
7. F. Morichetti, A. Melloni, C. Ferrari, and M. Martinelli, "Error-free continuously-tunable delay at 10 Gbit/s in a reconfigurable on-chip delay-line," Opt. Express **16**(12), 8395–8405 (2008).
8. N. Sherwood-Droz, H. Wang, L. Chen, B. G. Lee, A. Biberman, K. Bergman, and M. Lipson, "Optical 4x4 hitless slicon router for optical networks-on-chip (NoC)," Opt. Express **16**(20), 15915–15922 (2008).
9. M. H. Shih, W. J. Kim, W. Kuang, J. R. Cao, S.-J. Choi, J. D. O'Brien, and P. D. Dapkus, "Experimental characterization of the reflectance of 60° waveguide bends in photonic crystal waveguides," Appl. Phys. Lett. **86**(19), 191104 (2005).
10. M. Ayre, T. J. Karle, T. Lijun Wu, T. Davies, and T. F. Krauss, "Experimental verification of numerically optimized photonic crystal injector, Y-splitter, and bend," IEEE J. Sel. Areas Commun. **23**(7), 1390–1395 (2005).
11. I. Ntakis, P. Pottier, and R. M. De La Rue, "Optimization of transmission properties of two-dimensional photonic crystal channel waveguide bends through local lattice deformation," J. Appl. Phys. **96**(1), 12–18 (2004).
12. M. Lipson, "Guiding, modulating, and emitting light on Silicon – challenges and opportunities," J. Lightwave Technol. **23**(12), 4222–4238 (2005).
13. Y. A. Vlasov, and S. J. McNab, "Losses in single-mode silicon-on-insulator strip waveguides and bends," Opt. Express **12**(8), 1622–1631 (2004).
14. T. W. Ebbesen, C. Genet, and S. I. Bozhevolnyi, "Surface-plasmon circuitry," Phys. Today **61**(5), 44 (2008).
15. H. Raether, "Surface Plasmons on Smooth and Rough Surfaces and on Gratings," *Springer Tracts in Modern Physics* (Springer-Verlag, Berlin, 1988) Vol. 3.
16. P. Berini, "Plasmon-polariton waves guided by thin lossy metal films of finite width: Bound modes of symmetric structures," Phys. Rev. B **61**(15), 10484–10503 (2000).
17. D. K. Gramotnev, and D. F. P. Pile, "Single-mode subwavelength waveguide with channel plasmon-polaritons in triangular grooves on a metal surface," Appl. Phys. Lett. **85**(26), 6323–6325 (2004).

#128746 - $15.00 USD Received 20 May 2010; revised 21 Jun 2010; accepted 25 Jun 2010; published 15 Jul 2010

18. B. Steinberger, A. Hohenau, H. Ditlbacher, A. L. Stepanov, A. Drezet, F. R. Aussenegg, A. Leitner, and J. R. Krenn, "Dielectric stripes on gold as surface plasmon waveguides," Appl. Phys. Lett. **88**(9), 094104 (2006).
19. L. Chen, J. Shakya, and M. Lipson, "Subwavelength confinement in an integrated metal slot waveguide on silicon," Opt. Lett. **31**(14), 2133–2135 (2006).
20. J. A. Dionne, L. A. Sweatlock, H. A. Atwater, and A. Polman, "Plasmon slot waveguides: Towards chip-scale propagation with subwavelength-scale localization," Phys. Rev. B **73**(3), 035407 (2006).
21. M. Spasenović, D. van Oosten, E. Verhagen, and L. Kuipers, "Measurements of modal symmetry in subwavelength plasmonic slot waveguides," Appl. Phys. Lett. **95**(20), 203109 (2009).
22. J. Takahara, S. Yamagishi, H. Taki, A. Morimoto, and T. Kobayashi, "Guiding of a one-dimensional optical beam with nanometer diameter," Opt. Lett. **22**(7), 475–477 (1997).
23. S. I. Bozhevolnyi, V. S. Volkov, E. Devaux, J.-Y. Laluet, and T. W. Ebbesen, "Channel plasmon subwavelength waveguide components including interferometers and ring resonators," Nature **440**(7083), 508–511 (2006).
24. T. Holmgaard, Z. Chen, S. I. Bozhevolnyi, L. Markey, A. Dereux, A. V. Krasavin, and A. V. Zayats, "Bend- and splitting loss of dielectric-loaded surface plasmon-polariton waveguides," Opt. Express **16**(18), 13585–13592 (2008).
25. B. Steinberger, A. Hohenau, H. Ditlbacher, F. R. Aussenegg, A. Leitner, and J. R. Krenn, "Dielectric stripes on gold as surface plasmon waveguides: Bends and directional couplers," Appl. Phys. Lett. **91**(8), 081111 (2007).
26. M. I. Stockman, "Nanofocusing of optical energy in tapered plasmonic waveguides," Phys. Rev. Lett. **93**(13), 137404 (2004).
27. E. Verhagen, M. Spasenović, A. Polman, and L. K. Kuipers, "Nanowire plasmon excitation by adiabatic mode transformation," Phys. Rev. Lett. **102**(20), 203904 (2009).
28. M. L. M. Balistreri, J. P. Korterik, L. Kuipers, and N. F. van Hulst, "Phase mapping of optical fields in integrated optical waveguide structures," J. Lightwave Technol. **19**(8), 1169–1176 (2001).
29. M. Burresi, R. J. P. Engelen, A. Opheij, D. van Oosten, D. Mori, T. Baba, and L. Kuipers, "Observation of polarization singularities at the nanoscale," Phys. Rev. Lett. **102**(3), 033902 (2009).
30. Z. Zhu, and T. G. Brown, "Full-vectorial finite-difference analysis of microstructured optical fibers," Opt. Express **10**(17), 853–864 (2002).
31. E. A. Marcatili, "Bends in optical dielectric guides," Bell Syst. Tech. J. **48**, 2103 (1969).
32. R. G. Hunsperger, *Integrated Optics: Theory and Technology* (4th ed., Springer-Verlag, Berlin Heidelberg, 1995).

1. Introduction

In recent years, the generation and manipulation of subwavelength optical fields has become of great interest, because of potential applications in optical data processing [1], biophotonics [2], quantum [3] and nonlinear optics [4]. In the field of optical data processing, the integration of discrete photonic components on a chip has been a long-standing goal. Micrometer-scale waveguides, switches [5,6], delay lines [7], and routers [8] have been realized in various silicon-based materials. As more such components are fabricated on small areas, bending losses start to play an important role. Bending losses have been studied experimentally in photonic crystal [9–11], silicon [12], and silicon-on-insulator (SOI) [13] waveguides.

Recently, subwavelength confinement has been realized with surface plasmon polariton (SPP) optics [14], which could offer an alternative way to guide light on the submicron scale. Surface plasmon polaritons are electromagnetic surface waves coupled to charge oscillations at a metal-dielectric interface [15]. The evanescent field of SPPs typically extends a few hundred nanometers into the dielectric, and on the order of the skin depth (~10 nm) into the metal. This confinement to the metal-dielectric interface makes SPPs a natural candidate for the platform of choice in integrated optics. By using a strip of metal, plasmons can be confined to two-dimensional metal waveguides [16]. Further modifications of the number and shape of metal-dielectric interfaces resulted in high-confinement SPP waveguides, such as triangular wedges [17], dielectric stripes on metal [18], slot waveguides [19–21], and metallo-dielectric fiber waveguides [22]. Basic integrated plasmonic components such as interferometers and ring resonators have been successfully demonstrated in channel plasmon waveguides [23]. Transmission through S-shaped bends, splitters [24], and directional couplers [25] has been shown in dielectric stripes on metal. In addition metal nanowires can support guided plasmonic modes for arbitrarily small non-zero radii [22,26]. Verhagen et al. showed that such nanowires, with a width as small as 60 nm, can be fabricated on a chip and efficiently coupled to from the far field [27].

In this paper we present a study of bending losses in plasmonic nanowire waveguides. We use the adiabatic coupling scheme demonstrated in [27] to excite nanowire plasmon polaritons

#128746 - $15.00 USD Received 20 May 2010; revised 21 Jun 2010; accepted 25 Jun 2010; published 15 Jul 2010

(NPPs) on wires with widths of 70 nm and 40 nm. The NPPs propagate through bends with radii of curvature (R_C) ranging from 1 to 12 μm. With a phase- and polarization-sensitive near-field microscope we measure the electric field in the wire in both straight and curved segments. We determine the transmission through the bends as a function of R_C. We use the straight wire segments to measure propagation losses due to Ohmic damping and surface roughness, and then subtract that from the overall transmission losses in bends to reveal pure bending loss. Our data is supported by Finite Difference Time Domain (FDTD) modeling. A simple analytical model is used to describe the trend of the bending losses as a function of R_C.

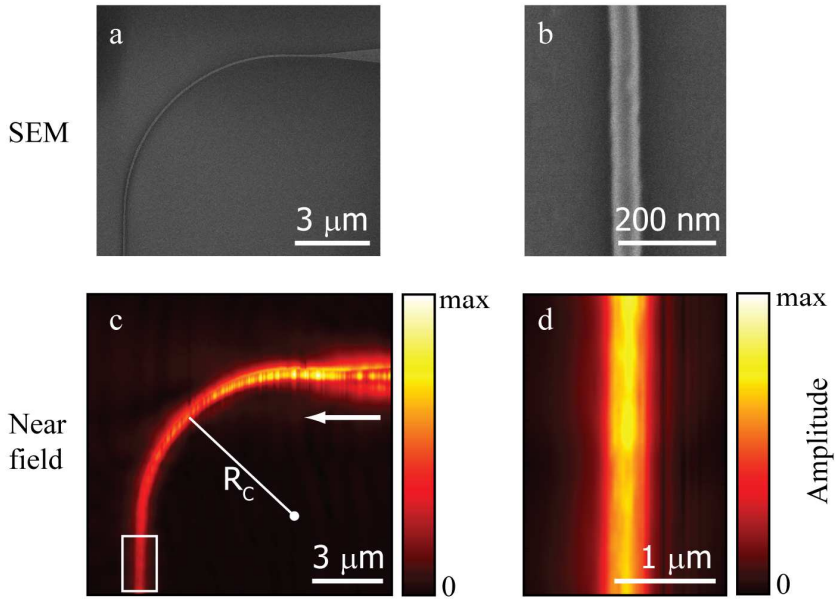

Fig. 1. Scanning electron micrographs (a and b) and measured near-field amplitudes (c and d) of straight (b and d) and curved (a and c) sections of a 70 nm wide nanowire waveguide. D is an enlargement of a straight section indicated with a white box in c. The radius of curvature of nanowires shown in a and c is 6 μm. The white arrow in c indicates the propagation direction of SPPs on the start of the nanowire bend. The colorbars show the time-averaged electric field amplitude, normalized to the largest measured signal.

2. Sample fabrication and near-field measurement

The gold nanowires are fabricated on a glass (BK-7) substrate using electron beam lithography. A 150 nm thick positive-resist layer (Zep520) is spin coated onto the substrate, after which a conductive polymer layer (necessary for electron beam exposure) is spin coated on top of the resist layer. After exposure the sample is developed in N-amyl acetate, removing all the exposed resist. A 50 nm thick gold layer is evaporated onto the substrate. The remaining resist and gold are chemically removed in a lift-off process, with N-Methylpyrrolidone. The designed structures consist of a grating of subwavelength holes, and a taper which is connected to a curved nanowire waveguide. The grating has a pitch of 1 μm. This pitch is chosen for the excitation of surface plasmon polaritons at the gold/glass interface, with a free-space wavelength λ_o = 1.55 μm. A beam of SPPs propagates into the tapered waveguide, and is adiabatically funneled to a nanowire [27]. The nanowire waveguides had a width of either 40 or 70 nm; as measured with a scanning electron

#128746 - $15.00 USD Received 20 May 2010; revised 21 Jun 2010; accepted 25 Jun 2010; published 15 Jul 2010

microscope (SEM). Figures 1(a) and 1(b) depict scanning electron micrographs of typical fabricated nanowire structures. Figure 1(b) depicts a straight nanowire section, with a width of 70 nm and Fig. 1(a) depicts a curved section with a radius of curvature of 6 μm. In all the investigated structures, the nanowire waveguides were designed to make a 90° bend with R_C ranging from 1 to 12 μm.

A phase- and polarization-sensitive near-field scanning optical microscope (NSOM) [28,29] was used to locally probe the electric field. The experiments were performed using an aluminum-coated near-field aperture probe, with aperture diameter of approximately 300nm. Figures 1(c) and 1(d) depict a measured near-field electric field amplitude for two different nanowire waveguide configurations: a straight waveguide section (d), and a curved waveguide with R_C = 6 μm (c). Figure 1(c) depicts SPPs approaching the nanowire from the right, propagating in the direction of the white arrow. We observe that the NPPs propagate along the curved nanowire waveguide without significant leakage of light around the bend.

3. Characterization of losses

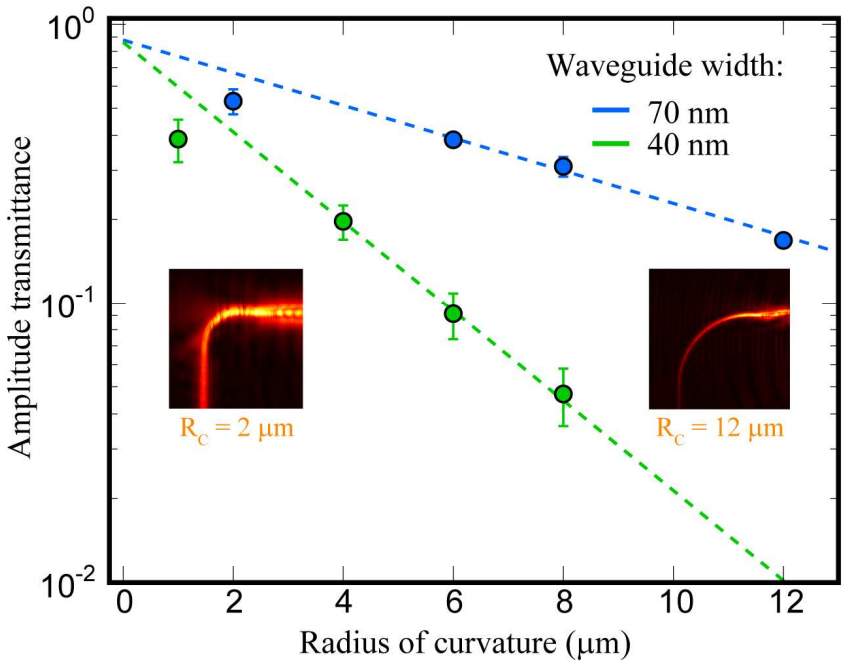

Fig. 2. Amplitude transmittance through a 90° bend as a function of radius of curvature. Blue and green points correspond to waveguides with widths of 70 nm and 40 nm, respectively. Dashed lines are exponential fits with a single exponent to the last three data points of the near-field amplitude transmittance measurements. The errorbars represent the experimental uncertainty. The insets show near-field amplitude images of two investigated structures.

3.1 Transmission through nanowire bends

Figure 2 shows the amplitude transmittance through curved nanowires with a width of 40 or 70 nm as a function of radius of curvature. The amplitude transmittance across the bend is determined by comparing the amplitude before and after a curve. The highest transmittance of 0.53 was observed in the case of a waveguide with a width of 70 nm and a radius of curvature of 2 μm. A general trend of decreasing transmission with increasing radius of curvature can be observed in all studied waveguides. For the general case of lossy waveguides, the intensity drops exponentially with the traversed path. A single exponentially decaying function is fitted to the last three data points in Fig. 2, shown as a dashed line. It is easily noticed that the data

#128746 - $15.00 USD Received 20 May 2010; revised 21 Jun 2010; accepted 25 Jun 2010; published 15 Jul 2010

point for the smallest R_C lies significantly beneath the fitted line in both cases, which indicates that for small R_C an additional loss component plays a role.

The simplest assumption is that the loss of the bends is governed by two exponentials, one for the propagation losses and one for the bending losses:

$$A_{out} / A_{in} = \exp\left(-k''_{propagation} x\right) \cdot \exp\left(-k''_{bending} x\right). \quad (1)$$

In Eq. (1), $k''_{propagation}$ represents the attenuation of the electric field per unit length due to propagation losses, $k''_{bending}$ represents the attenuation due to bending losses, and x is the length along the waveguide. A_{out}/A_{in} is the amplitude transmittance around the bend, which can also be expressed as $\exp(-k''_{total}x)$, where k''_{total} is the total attenuation of the electric field per unit length through the bend.

3.2 Propagation losses

In the case of plasmonic structures, propagation losses generally consist of both Ohmic and scattering components. Ohmic losses are due to power dissipated by scattering of electrons inside the metal. Scattering losses are the conversion of power from the propagating mode to free radiation by scattering from surface or bulk imperfections. Both components are present in straight, as well as curved nanowire sections.

Comparing the slopes of the fits for the two different waveguide widths in Fig. 2, we observe that the transmission in a 40 nm wide nanowire decreases faster with increasing R_C. In contrast to the case of a dielectric waveguide, where the mode is gradually expelled as the guide is narrowed, in the case of nanowire plasmons the mode retracts into the wire as it gets narrower [22,26,27]. Consequently, in narrower waveguides a larger fraction of the mode resides in the metal and hence Ohmic losses are higher than in wider wires. By fitting a decaying exponential function to the amplitude in straight nanowire sections, we obtain average values of $k''_{propagation} = 0.2 \pm 0.05\ \mu m^{-1}$ in 40 nm wide waveguides, and $k''_{propagation} = 0.085 \pm 0.006\ \mu m^{-1}$ in 70 nm wide waveguides. As expected, the propagation attenuation is smaller in the wider waveguide.

3.3 Isolating the bending losses

From Eq. (1) and the presented data, we can extract a value for $k''_{bending}$ by substituting x by $R_C\pi/2$ (the path traversed in a 90° bend). This yields

$$k''_{bending} = -\log\left(\frac{A_{out}}{A_{in}}\right)\frac{2}{\pi R_C} - k''_{propagation}. \quad (2)$$

In the above equation, we have made the assumption that propagation losses are the same in straight sections of the waveguide as in the curved sections. The assumption is verified with FDTD simulations, which show that the mode profile does not change significantly even in bends with small R_C. A similar mode profile lets us assume that the surface scattering losses are the same for straight and curved waveguide sections. Ohmic losses and bulk scattering losses stay the same, irrespective of bending radius. Figure 3(a) depicts the measured attenuation in 70 nm wide waveguides. The total attenuation (k''_{total}) is measured as described in section 3.1, the propagation attenuation ($k''_{propagation}$) as described in section 3.2, after which $k''_{bending}$ is extracted according to Eq. (2). The rise in attenuation (green circles) for small R_C in Fig. 3(a) corresponds to the drop in amplitude transmittance seen in Fig. 2. Propagation losses (blue circles) remain constant for all waveguides with the same width, apart from small fluctuations, which we attribute to small variations in the width of wires for different realizations. As a result, the attenuation due to bending (orange circles) increases as R_C decreases. At radii of curvature larger than ~6 μm, bending losses are negligible compared to propagation losses, however at radii smaller than ~4 μm the two loss mechanisms become comparable in magnitude. At curvatures with radii smaller than ~2 μm, bending losses appear to become dominant.

#128746 - $15.00 USD Received 20 May 2010; revised 21 Jun 2010; accepted 25 Jun 2010; published 15 Jul 2010

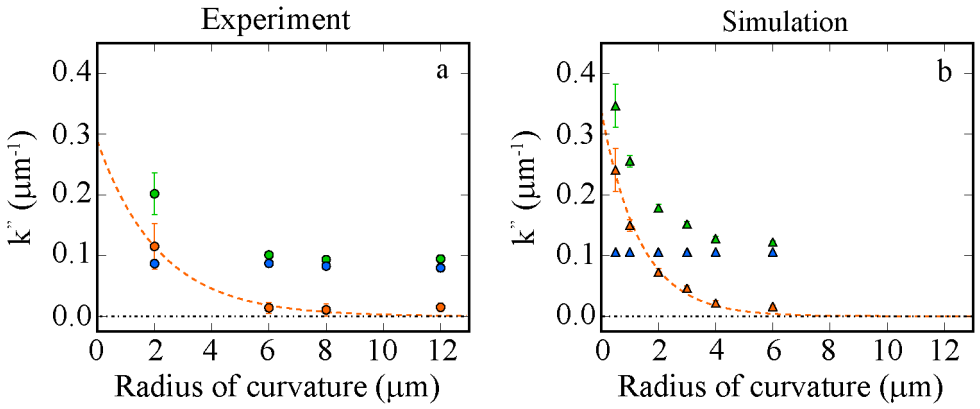

Fig. 3. Attenuation due to bending losses obtained for waveguides with a width of 70 nm. a: experimentally obtained values for k''_{total} (green), $k''_{propagation}$ (blue) and $k''_{bending}$ (orange). b: Attenuation values obtained from FDTD simulations. The dashed orange lines indicate the fit to an exponential function. The error bars in the left image represent experimental uncertainty. In the right image, the error bars represent the uncertainty in placing power monitors exactly at the beginning and end of a bend.

3.4 Simulation

We compare the experimental results to FDTD simulations with a commercial simulation software (Lumerical FDTD Solutions v6.5.11). The substrate was modeled as a uniform slab of BK7, with refractive index 1.50066. The permittivity of gold was fitted to a Drude model, around a wavelength of 1.55 μm using optical constants obtained from ellipsometry measurements performed on a similar sample. Perfectly matched layers (PML) were employed around the simulation box to absorb radiated power. The wire cross-section was modeled as a rectangle with a width of 70 nm and a height of 50 nm. A finite difference frequency domain solver, described in reference [30], was used to obtain the mode profile that is used as the excitation source at the intersection of the nanowire with the simulation boundary. The mode has the highest intensity at the surface of the gold wire, which results in strong electric field gradients, especially at the nanowire corners. To ensure that we capture the gradient with sufficient resolution, the mesh size was varied from 10 nm down to 1 nm, while monitoring amplitude transmittance of a straight section of the waveguide. No noticeable change in transmittance occurred while reducing the mesh size from 2 nm to 1 nm. In the final simulation, we used a size of 2 nm for the smallest elements of the simulation mesh. To check whether the absorption of the evanescent tail by the PML affects the results, we varied the size of the simulation box. A distance of 1.2 μm between the structure and the PML was found to be sufficient to obtain reliable results.

The results of the FDTD simulation are shown in Fig. 3(b). Similar to experimental results, the total attenuation (green triangles) rises with decreasing radius of curvature. The attenuation due to bending losses (orange triangles) rises with decreasing R_C, becoming the dominant loss component at a radius of curvature below 2 μm.

4. Discussion

A simple model to describe radiation loss in bends leads to bending losses that depend exponentially on the radius of curvature R_C [31]:

$$k''_{\text{bending}} = C_1 \exp\left(-C_2 R_C\right), \text{ where } C_2 = \beta\left(2\Delta n_{eff}/n_{eff}\right)^{3/2}, \qquad (3)$$

C_1 depends on the dimensions of the waveguide, β is the propagation constant of the mode, and Δn_{eff} is the difference between the modal effective index n_{eff} and the index of the surroundings. Equation (3) was derived for dielectric slab waveguides [32], for which electric

#128746 - $15.00 USD Received 20 May 2010; revised 21 Jun 2010; accepted 25 Jun 2010; published 15 Jul 2010

field intensity decays exponentially outside of the waveguide. In a waveguide curve, at a certain distance X_o away from the center of the waveguide, the wavevector of the guided light matches that of light freely propagating in the surroundings. The bending losses of the waveguide scale with the fraction of the total modal energy beyond this distance X_o. This leads to exponentially decreasing losses with increasing R_C, as in Eq. (3). In the curved plasmonic nanowires considered in this work, the mode has an effective index slightly higher than that of the glass substrate, hence in a bend the energy primarily leaks into the glass, and not the air. To verify that Eq. (3) is valid in plasmonic nanowire waveguides, we perform simulations to show that the electric field intensity in the substrate decays exponentially outside of the waveguide. In Fig. 4 we show the fraction of the total energy which lies in the glass substrate, outside a distance X away from the center of the waveguide, for straight nanowires with widths of 40 nm and 70 nm. The blue and green data points were obtained from a numerical mode solver (COMSOL). The overlaid red lines are exponential fits. In both cases, the exponential fit matches well to the numerical data, especially at distances close to the waveguide, where most of the energy resides. This observation shows that the assumption underlying Eq. (3) is fulfilled for NPPs just like for dielectric waveguides. We therefore fit Eq. (3) to the experimental and simulated data, shown as dashed orange lines in Fig. 3. Table 1 displays the resultant fit coefficients.

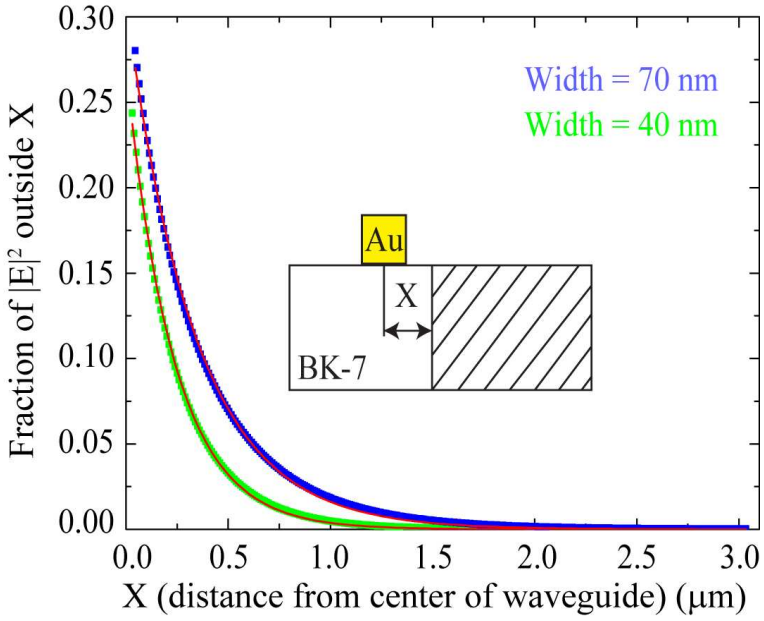

Fig. 4. The fraction of energy in the substrate. BK-7 is the glass substrate, Au is the gold nanowire. X is the distance from the center of the nanowire waveguide. The green and blue dots are results of numerical simulations for wires of width 40 nm and 70 nm, respectively. The shaded area of the substrate marks the area from which the fraction is calculated. An exponentially decaying dependence on X is observed, which is confirmed with overlaid exponential fits (red lines).

#128746 - $15.00 USD Received 20 May 2010; revised 21 Jun 2010; accepted 25 Jun 2010; published 15 Jul 2010

Table 1. Coefficients obtained by fitting to Eq. (3)

	C_1 [μm^{-1}]	C_2 [μm^{-1}]
Experiment (70 nm)	0.289 ± 0.081	0.461 ± 0.140
FDTD simulation (70 nm)	0.348 ± 0.015	0.752 ± 0.048
Experiment (40 nm)	0.638 ± 0.077	0.457 ± 0.096
FDTD simulation (40 nm)	0.361 ± 0.041	1.040 ± 0.012

At a free-space wavelength of 1.55 μm and for a nanowire width smaller than ~200 nm, the effective mode index rises with decreasing width [27]. As a result, plasmons are better confined to narrower wires (see Fig. 4) and the simulated C_2 is higher at a width of 40 nm than at 70 nm, which results in smaller bending losses. The simulated C_1 is equal for the two widths, which is not surprising since the difference in waveguide widths in the two cases is small. The values extracted from experiments are close to simulation results, although the absolute numbers do not match. As the bending losses become the dominant loss mechanism for only the smallest of the measured R_C, more measurements at radii below 1 micrometer would be required to find the combination of C1 and C2 that describes the bending losses best.

The effective index in plasmonic nanowires with a width of 40 nm is only slightly higher than the index in the underlying glass substrate, whereas the index contrast in dielectric waveguides can be significantly higher [13]. Higher index contrast in dielectrics allows for smaller bending losses at similar radii of curvature [11,13]. Nevertheless, plasmonic nanowires have smaller footprints and allow for more densely stacked waveguides. Additionally, the effective index in nanowires is predicted to be larger for smaller waveguide widths, and also when the dielectric surrounding is symmetric. This may therefore allow reduction of bending losses at comparable mode confinement.

5. Conclusion

In conclusion, propagation losses and bending losses were measured in plasmonic nanowire waveguides with widths of 40 nm and 70 nm. Using a near-field microscope, amplitude transmittances of up to 0.5 were measured in 70 nm wide nanowires with a radius of curvature of 2 μm. Bending losses were isolated from propagation losses. The amplitude attenuation due to bending was found to be as small as 0.1 μm^{-1} in the same wire. Measurements were supported by FDTD simulations. An analytical model developed for dielectric waveguides is employed to describe the losses, which exponentially decay as a function of the radius of curvature. Further improvements in the fabrication procedure could decrease bending losses by generating narrower wires.

Acknowledgments

The authors would like to thank C. Rétif for the development of the fabrication procedure using a positive resist. This work was made possible by the facilities of the Amsterdam nanoCenter. This work is part of the research program of the Stichting voor Fundamenteel Onderzoek der Materie (FOM), which is financially supported by the Joint Solar Programme (JSP) of FOM, which is cofinanced by Gebied Chemische Wetenschappen of NWO and Stichting Shell Research. We acknowledge the support of the EC under the Marie Curie Scheme (Contract No. MEST-CT-2005-021000).

#128746 - $15.00 USD Received 20 May 2010; revised 21 Jun 2010; accepted 25 Jun 2010; published 15 Jul 2010